HHS Public Access

Author manuscript

Nat Neurosci. Author manuscript; available in PMC 2015 November 01.

Published in final edited form as:

Nat Neurosci. 2015 May ; 18(5): 683–689. doi:10.1038/nn.3992.

Neuronal activity biases axon selection for myelination in vivo

Jacob H. Hines[1,2], **Andrew M. Ravanelli**[1], **Rani Schwindt**[1], **Ethan K. Scott**[3], and **Bruce Appel**[1]

[1]Department of Pediatrics, University of Colorado School of Medicine, Aurora CO 80045

[3]School of Biomedical Sciences, The University of Queensland, St. Lucia, QLD, Australia

Abstract

An essential feature of vertebrate neural development is ensheathment of axons with myelin, an insulating membrane formed by oligodendrocytes. Not all axons are myelinated, but mechanisms directing myelination of specific axons are unknown. Using zebrafish we show that activity-dependent secretion stabilizes myelin sheath formation on select axons. When VAMP2-dependent exocytosis is silenced in single axons, oligodendrocytes preferentially ensheath neighboring axons. Nascent sheaths formed on silenced axons are shorter in length, but when activity of neighboring axons is also suppressed, inhibition of sheath growth is relieved. Using in vivo time-lapse microscopy, we show that only 25% of oligodendrocyte processes that initiate axon wrapping are stabilized during normal development, and that initiation does not require activity. Instead, oligodendrocyte processes wrapping silenced axons are retracted more frequently. We propose that axon selection for myelination results from excessive and indiscriminate initiation of wrapping followed by refinement that is biased by activity-dependent secretion from axons.

In the developing central nervous system (CNS), oligodendrocytes extend membrane processes that ensheath axons with a lipid-rich myelin membrane. Myelination enables thinner axons to transmit information more rapidly, facilitating evolution of a complex yet compact CNS in vertebrate animals. Despite this advantage, not all axons are myelinated. For instance, in the corpus callosum, a major white-matter tract connecting cerebral hemispheres, fewer than half of all axons become myelinated[1]. Although selective mechanisms clearly exist in vivo, cultured oligodendrocytes will myelinate fixed axons or synthetic fibers with a diameter larger than 0.4 μm[2,3]. If axon diameter is sufficient for indiscriminate myelination in vitro, what mechanisms enable oligodendrocytes to make stereotyped decisions and myelinate specific axons in vivo?

Correspondence should be addressed to J.H.H. (jhhines@winona.edu) or B.A. (bruce.appel@ucdenver.edu).

[2]Present address: Biology Department, Winona State University, Winona MN 55987.

Author Contributions

JHH and BA conceived the project. JHH generated all new transgenic zebrafish lines and performed fluorescence microscopy experiments. AMR cloned the zebrafish *phox2B* promoter and performed veratridine and Channelrhodopsin experiments. RS performed electron microscopy experiments and assisted with cell count experiments. ES produced the *Tg(UAS:Syn-GFP)* transgenic line. JHH wrote and BA edited the manuscript.

Numerous studies show that electrical activity promotes myelination[4–9], raising the possibility that action potentials and release of axonal factors instruct nearby oligodendrocyte processes to initiate ensheathment. Unmyelinated axons secrete neurotransmitters and neurotrophic factors extrasynaptically along axons[10–12], and pre-myelinating oligodendrocytes express a plethora of receptors that are poised to interpret axonal factors released in response to activity[13]. Consistent with this possibility, electrical stimulation of cultured neurons triggers local Ca^{2+} signaling in oligodendrocyte processes, which requires synaptic vesicle exocytosis and glutamate receptors[7]. The mechanisms mediating axon selection in vivo, and the contribution of neuronal activity, remain completely unknown.

The inability to visualize and genetically manipulate subsets of axons in vivo, while simultaneously visualizing which axons are ensheathed by oligodendrocyte wrapping processes, has precluded the discovery of axon selection mechanisms. Here, we have investigated oligodendrocyte membrane sheath formation on single, identifiable axons under normal and electrically silenced conditions in zebrafish larvae. We found that the majority of oligodendrocyte membrane processes in ventral spinal cord tracts select and ensheath *phox2B*$^{+}$ axons. The fidelity of this axon choice was reduced when VAMP2-dependent exocytosis or electrical excitability was suppressed in single axons, indicating that axon selection is biased by activity-dependent secretion. Moreover, myelin sheaths that did form on single silenced axons were shorter in length. This activity-dependent control of sheath length is influenced by other axons, because suppressing all electrical activity restored normal sheath length. Finally, using in vivo time-lapse microscopy we found that oligodendrocytes wrapping silenced axons retract sheaths more frequently. Collectively, this study raises a new model for axon selection whereby oligodendrocytes initially form excess sheaths, detect differences in activity-dependent secretion between ensheathed axons, and preferentially maintain sheaths on select axons. These findings extend recent discoveries that social experiences and experimentally altered neuronal activity can influence oligodendrocyte proliferation, differentiation and myelin sheath thickness[9,14,15] by demonstrating that neuronal activity can bias which axons become myelinated, an additional means of myelin plasticity. Additionally, our work indicates that molecular and cellular mechanisms that stabilize myelin sheaths following indiscriminate sheath initiation contribute importantly to axon selection in response to activity.

RESULTS

Activity-dependent secretion regulates axon selection

We have developed a genetically tractable system to study mechanisms of axon selection in the zebrafish spinal cord. Testing the activity-dependent myelination hypothesis in vivo necessitated transgenic reporters permitting direct observation of subsets of myelin-fated axons, and drivers enabling genetic manipulation of neuronal activity. In *Tg(phox2B:GFP)* zebrafish larvae (hereafter *phox2B*:GFP), a subset of hindbrain neurons with axons projecting into ventral spinal cord tracts express GFP (Supplementary Fig. 1). In transverse spinal cord sections, *phox2B*$^{+}$ axons were surrounded by myelin basic protein (MBP), a marker for myelin sheaths (Supplementary Fig. 1). To observe the initial myelination of

phox2B^{+} axons in live zebrafish, we visualized nascent sheaths by confocal microscopy using the *Tg(sox10:mRFP)* reporter, which expresses membrane-tethered RFP in oligodendrocyte lineage cells (hereafter *sox10*:mRFP). *phox2B*$^{+}$ axons were ensheathed shortly after the onset of myelination, and a majority of nascent sheaths in the ventral spinal cord wrapped *phox2B*$^{+}$ axons (Fig. 1a). If axon selection requires electrical activity, then suppressing activity should abrogate the selection of myelin-fated *phox2B*$^{+}$ axons. To test this, we treated *phox2B*:GFP; *sox10*:mRFP larvae with the voltage-gated sodium channel blocker tetrodotoxin (TTX) at 48 hours post fertilization (hpf), prior to the onset of myelination. TTX treatment paralyzed zebrafish larvae for at least three days without major developmental defects or toxicity, but did not prevent myelin sheath formation in the spinal cord. We assessed axon selection in *phox2B*:GFP; *sox10*:mRFP reporter larvae and found that TTX treatment reduced the proportion of nascent sheaths wrapping *phox2B*$^{+}$ axons (Fig. 1a,b). In contrast, TTX treatment had no effect on the overall number or length of nascent sheaths (Fig. 1c,d), or the number of spinal cord oligodendrocyte progenitor cells or oligodendrocytes (Supplementary Fig. 2). Together, these data show that TTX-sensitive activity is not required for oligodendrocyte differentiation or formation of nascent sheaths in vivo, but biases axon choice.

If activity is necessary for biased axon choice, can heightened activity enhance wrapping? To test this we treated embryos with the Na^{+} channel modulator veratridine at 72 hpf, immediately prior to the onset of myelination. Veratridine prolongs Na^{+} channel opening and, as expected, injected embryos showed striking and sustained behavioral phenotypes. Upon touch stimulation, control embryos initiated short bursts of swim movements (Supplementary Video 1). By contrast, veratridine-treated embryos initiated a prolonged swim response that eventually terminated in seizure-like behavior and brief paralysis (Supplementary Video 2). Although veratridine treatment had a pronounced effect on neural behavior (Fig. 2a), we observed no change within the spinal cord in the selection of *phox2B*$^{+}$ axons or the overall level of wrapping (Fig. 2b–d). However, the length of nascent sheaths on both *phox2B*$^{+}$ and *phox2B*$^{-}$ axons was slightly reduced in veratridine-treated embryos relative to controls (Fig. 2e). We conclude that TTX-sensitive activity is necessary for selection of axons at high fidelity but that widespread elevated neuronal activity is not sufficient to increase wrapping of spinal cord axons.

To test whether activity-dependent signals that bias axon choice originate in neurons, we next inhibited synaptic vesicle exocytosis selectively in *phox2B*$^{+}$ axons by targeted overexpression of tetanus neurotoxin (TeNT), a protease that cleaves select Vesicle-Associated Membrane Protein (VAMP) family proteins including Synaptobrevin/VAMP2. This is a potent inhibitor of synaptic vesicle exocytosis in many animal models including zebrafish[16,17]. We cloned a 2.1 kb genomic fragment of the zebrafish *phox2B* gene and generated the *Tg(phox2B:GAL4)* line. When crossed to *Tg(UAS:mCherry-CaaX)*, mCherry was faithfully co-expressed in axons marked by *phox2B:*GFP, validating the specificity of this new transgenic line (Supplementary Fig. 1). We injected *Tg(phox2B:GAL4)* embryos at early cleavage stage with DNA plasmids encoding *UAS*:GFP or *UAS*:TeNT-GFP, resulting in mosaic expression in single *phox2B*$^{+}$ axons of 4-day larvae. When *phox2B*$^{+}$ axons expressed GFP as a control, 55.3% were myelinated at the time of imaging, whereas only

31.6% expressing TeNT-GFP were myelinated (Fig. 3a,b). Quantitatively, we found that single TeNT-GFP$^+$ axons were less well wrapped, because the percent length of axons ensheathed by *sox10:*mRFP$^+$ sheaths was reduced (Fig. 3c). Notably, when oligodendrocytes did wrap TeNT-GFP$^+$ axons, nascent sheaths were shorter in length (Fig. 3d).

Our finding that nascent sheath length is reduced on single TeNT-GFP$^+$ axons but unaffected when all axons are silenced by TTX is reminiscent of competition mechanisms that refine topographic maps in the visual system[16,18–20]. To test for activity-based interactions among axons that could modulate myelination, we next asked whether the effects of blocking vesicular release are influenced, or rescued, when neighboring axons are also silenced. We treated larvae with single *UAS:*TeNT-GFP$^+$ axons with TTX to suppress activity in surrounding axons. In comparison to single TeNT-GFP$^+$ axons in a normal environment, nascent sheaths wrapping TeNT-GFP$^+$ axons in TTX-treated larvae grew to their usual lengths (Fig. 3d). However, only 21.4% of TeNT-GFP$^+$ axons were selected for myelination, and the overall ensheathment of *phox2B*$^+$ axons remained reduced (Fig. 3b,c). These findings demonstrate that control of nascent sheath length involves vesicular release and is influenced by neighboring axons. In addition, the observation that *phox2B*$^+$ axons remain selected with reduced fidelity when activity in other axons is suppressed suggests that additional activity-dependent, non-competitive forces participate in axon selection.

To test the requirement for neuronal excitability in axon selection we used targeted overexpression of the inward rectifier K$^+$ channel Kir2.1 in single *phox2B*$^+$ axons. This approach suppresses neuronal excitability in various model systems including zebrafish neurons[18,21,22]. In axon selection assays, *UAS:*Kir2.1-2A-GFP$^+$ axons were selected for myelination less frequently than controls (Fig. 3b,c). However, unlike TeNT-GFP$^+$ axons, nascent sheaths wrapping Kir2.1-2A-GFP$^+$ axons were normal in length (Fig. 3d). Collectively, these data reveal distinct activity-dependent forces during axon selection. Synaptic vesicle release biases axon selection and positively regulates myelin sheath length in a manner that can be influenced by activity in other axons. Additional forces mediated by excitability, which are suppressed by TTX and Kir2.1 but not influenced by activity in other axons, are also required for axon selection. Notably, myelin sheath length is reduced on single TeNT-GFP$^+$ axons that are excitable but cannot perform VAMP2-dependent exocytosis, whereas sheath length is normal on Kir2.1-2A-GFP$^+$ axons with reduced excitability but normal exocytic function.

We next asked whether ectopic neuronal activity in *phox2B*$^+$ is sufficient to modulate axon selection and initial ensheathment by crossing *Tg(phox2B:GAL4)* to the *Tg(UAS:ChRWR-EGFP)* line, which can induce activity of zebrafish spinal neurons in response to blue light stimulation[23]. Prior to optogenetic stimulation, we performed confocal microscopy to identify the specific somite at which oligodendrocytes were initiating ensheathment. After blue light stimulation (473 nm), we returned to the same position and found no change in the proportion of wrapped *phox2B*$^+$ axons or the overall ensheathment of *phox2B*$^+$ axons after 24 hours (Supplementary Fig. 3). These data are consistent with our pharmacologic stimulation (Fig. 2), further indicating that ectopic neuronal activity in *phox2B*$^+$ axons is not sufficient to alter selection or ensheathment. However, we cannot rule out the possibility that

an undetermined stimulation pattern within *phox2B*$^+$ axons could bias axon selection or regulate ensheathment.

Our observation that vesicle release from axons regulates selection for myelination raises the possibility that vesicle cargo is locally secreted from axons onto oligodendrocyte processes, acting instructively to initiate or maintain nascent sheaths. We next performed confocal microscopy to directly observe the distribution and behavior of axonal vesicles at and away from sites of ensheathment. When *Tg(phox2B:GAL4)* was crossed to *Tg(UAS:Synaptophysin-GFP)* (hereafter *UAS:*Syn-GFP) we observed single labeled axons containing vesicles marked by GFP (Fig. 4, Supplementary Video 3). Vesicle puncta were both stationary and motile, with rates of movement consistent with microtubule-based axonal transport. When crossed to the *Tg(sox10:mRFP)* transgenic reporter, we frequently found accumulations of Syn-GFP$^+$ vesicle puncta at sites of ensheathment (Fig. 4a). Syn-GFP$^+$ puncta at ensheathment sites may be represent a stable vesicle pool, or could be undergoing transport toward or away from the synaptic terminal. To distinguish between these possibilities, we collected time-lapse images at 10 s intervals and measured the motility of vesicles at unmyelinated segments and ensheathment sites. Whereas Syn-GFP$^+$ puncta at unmyelinated segments were frequently motile, vesicle puncta at ensheathment sites were typically stationary (Fig. 4b,c). Taken together, these data are consistent with the possibility that axon secretion at ensheathment sites participates in axon selection.

Axon secretion is required for myelin sheath maintenance

What are the neuron-oligodendrocyte interactions leading to the preferential myelination of specific axons? We next aimed to determine whether axon secretion regulates myelination before or after initial ensheathment. In a preferential ensheathment model, axons without the proper excitability and secreted factors will not support initial ensheathment. Alternatively, in a preferential maintenance model, silenced axons can be initially wrapped but will not maintain sheaths. To test the contribution of activity-dependent secretion in these models, we generated the transgenic line *Tg(neuroD:TeNT-GFP)*. In this line, the pan-neuronal driver *neuroD* expresses TeNT-GFP broadly in neurons but not oligodendrocytes (Supplementary Fig. 4). Consequently, *Tg(neuroD:TeNT-GFP)* larvae (hereafter *neuroD:*TeNT) show no spontaneous locomotion or touch response (Supplementary Video 4). *neuroD:*TeNT expression, which is initiated prior to oligodendrocyte progenitor cell specification, caused a slight reduction in oligodendrocyte progenitor cell and oligodendrocyte numbers (Supplementary Fig. 5), similar to observations describing in an accompanying manuscript (Mensch et al.). Because TTX treatments, initiated after formation of oligodendrocyte lineage cells, had no effect on cell number, we conclude that activity promotes specification. Oligodendrocytes in *neuroD:*TeNT$^+$ larvae do form nascent sheaths (Figs. 5a and Supplementary Fig. 5), further supporting our conclusion that neuronal activity and synaptic vesicle exocytosis are not required for initial ensheathment of axons in vivo. Moreover, electron micrographs showed no difference in axon diameter between wild-type and *Tg(neuroD:TeNT-GFP)* larvae (Supplementary Fig. 6), suggesting that phenotypes resulting from TeNT-GFP overexpression are due to inhibition of exocytosis rather than a change in axon diameter.

To test the preferential ensheathment model, we performed time-lapse microscopy to assess oligodendrocyte membrane sheath initiation and stability in *neuroD:*TeNT^{+} larvae. We used the *Tg(sox10:mRFP)* reporter to observe initial axon wrapping attempts using an imaging paradigm with greater temporal resolution than previous studies. Remarkably, this revealed an unanticipated frequency of failed ensheathments in all samples (see examples in Supplementary Video 5). In both sibling control and *neuroD:*TeNT^{+} larvae, ~ 75% of wrapping attempts, or prospective sheaths, had disappeared within 90 min. Thus, 25% of prospective sheaths wrapping normal or silenced axons were initially stabilized in either condition, arguing against the preferential ensheathment model (Fig. 5a,b; Supplementary Videos 6–9). Intriguingly, although the proportion of wrapping attempts initially stabilized was unaffected, the ensheathment failure occurred more rapidly when prospective sheaths attempted to wrap silenced axons (Fig. 5c).

To test the preferential maintenance model, we next performed time-lapse microscopy to visualize the fate of pre-existing sheaths over an extended time period. We again utilized *Tg(neuroD:TeNT-GFP)*; *Tg(sox10:mRFP)* larvae, imaging at 20 min intervals to track individual oligodendrocyte membrane sheaths over a 15-hr period. We focused on sheaths that had initiated several hours prior, and similar to previous reports[24], found that existing sheaths were extremely stable. Whereas retractions were rare in control larvae, sheaths were retracted more frequently in *neuroD:*TeNT^{+} larvae (Fig. 6a,b; Supplementary Videos 10–11). In both conditions, sheaths that retracted were initially shorter than stable sheaths (Fig. 6c). Also consistent with the preferential maintenance model, and with the findings of Mensch et al. (accompanying paper), we found that by 5 dpf, singly-labeled oligodendrocytes in *neuroD:*TeNT^{+} larvae possessed fewer sheaths (Supplementary Fig. 5). Time-lapse imaging of singly-labeled oligodendrocytes in *neuroD:*TeNT^{+} larvae also supported a relationship between sheath length and retraction. Within three hours of initiation, prospective sheaths that were later maintained had extended more rapidly and were longer in length. In contrast, prospective sheaths that would be retracted extended more slowly, and never exceeded 10 μm in length before being retracted (Supplementary Fig. 7a–c). Collectively, our in vivo time-lapse imaging experiments demonstrate that the maintenance of nascent sheaths is regulated by activity-dependent secretion from axons, whereas initial axon wrapping is activity-independent.

DISCUSSION

Taken together, our findings raise a model whereby after initial axon wrapping, activity-dependent secretion from axons promotes extension and stabilization of prospective sheaths. In the absence of this input, oligodendrocyte membrane sheaths could form but did not extend, and were retracted at a higher frequency. Oligodendrocytes sampled many axons during the first several hours after initiating myelination, but 75% of initial wrapping segments failed to form stable sheaths. In an environment in which all axons are excitable, VAMP2-dependent secretion from axons promotes myelin sheath growth, and our time-lapse imaging indicated that shorter sheaths are more susceptible to subsequent retractions. In this way, excess axon wrapping is refined, and specific axons preferentially maintain myelin sheaths. This highlights a major gap in our current knowledge. If all axons secrete

neurotransmitters upon spontaneous and evoked activity, what are the specific factors that distinguish myelin-fated axons from those that will never be myelinated?

Our findings that activity and synaptic vesicle release bias axon selection provide insight into a critical facet of neural development with no previously known mechanism. In culture, oligodendrocytes can myelinate fixed axons and synthetic materials greater than 0.4 μm in diameter[2,3]. A minimal diameter may be permissive for myelination, but cannot explain how stereotyped decisions to myelinate occur in vivo. Does axon diameter act instructively prior to ensheathment and specify axons for myelination? Electron microscopy studies show a strong correlation between axon diameter and myelination. In the corpus callosum, 80% of myelinated axons have a diameter > 0.4 μm. Yet, there is considerable overlap between the diameters of myelinated and unmyelinated axons, suggesting that axon caliber alone is not sufficient to trigger myelination[1]. In the absence of causal evidence that axon diameter acts instructively, an alternative possibility is that a minimal diameter of 0.3–0.4 μm is permissive for initial ensheathment, followed by radial growth to increase axon diameter[1,25,26]. Because axon diameter was unaffected by TeNT-GFP overexpression, we conclude that activity-dependent secretion biases axon choice independently of axon diameter.

Our data are consistent with previous reports that oligodendrocytes have a brief window of myelinogenic potential[24]. The closure of this developmental window does not involve neuronal activity, because after several hours of initial axon wrapping, oligodendrocytes did not form new sheaths in *Tg(neuroD:TeNT-GFP)* larvae (see Supplementary Fig. 7d). Is activity-dependent refinement solely responsible for determining which axons are myelinated? Others have suggested that the amount of myelin pruning is insufficient to eliminate all excess or spurious initial wrapping, and have proposed that unidentified mechanisms may specify which axons can be wrapped prior to ensheathment[27]. Our data do not exclude the possibility that activity-independent forces also contribute to axon selection prior to initial ensheathment. Such mechanisms seem likely given our findings that *phox2B*$^{+}$ axons can still be ensheathed, albeit at a lower frequency, in the presence of TTX or tetanus neurotoxin.

How might new or enhanced brain activity stimulate myelination in vivo? Mice running on a wheel with complex rung spacing increase production of oligodendrocytes[28] and optogenetic stimulation, within the physiological range, promotes proliferation and maturation of oligodendrocyte lineage cells and myelin thickness[9]. Additionally, an accompanying study (Mensch et al.) shows that pharmacologically induced brain activity can promote formation of excess myelin sheaths by individual oligodendrocytes in zebrafish. By contrast, our optogenetic and pharmacological manipulations did not overtly change axon wrapping or axon selection bias in zebrafish spinal cord. One possible explanation is that mechanisms that mediate axon selection require highly specific activity codes that were not replicated in our gain of function experiments. Alternatively, activity might not be sufficient to direct myelination of axons that normally remain unmyelinated or to induce myelination prematurely. Because all axons are active, axon selection mechanisms that do not rely solely on activity would prevent ectopic myelination, which could be

detrimental. Instead, activity might enhance myelination of predetermined axons, thereby strengthening specific neural circuits in response to experience.

Whether electrical activity and neurotransmitter release regulates myelination is a long-standing question with conflicting results[6,7,29,30]. Our findings are consistent with models of activity-dependent regulation of myelination and highlight specific roles in axon selection and myelin sheath maintenance. Might neuronal activity influence axon selection via mechanisms resembling synaptogenesis[27]? Substantial evidence supports extrasynaptic release of axonal factors such as glutamate at sites of oligodendrocyte contact[10,11], and our own data show vesicle accumulation at ensheathment sites. This, coupled with evidence for membrane potential shifts and action potential-induced Ca^{2+} signaling in processes of oligodendrocyte-lineage cells[7,31,32], supports a model where axon-oligodendrocyte interactions along the axon locally regulate myelination in response to neuronal activity.

Myelination greatly impacts action potential conduction velocity, and in principle, activity-dependent myelination has profound implications for spike timing and Hebbian learning. Therefore, myelination of specific axons, and the parameters of this myelin, may be especially important for normal brain function. Supporting this notion, many neuropsychiatric disorders have been linked to myelin genes and white matter abnormalities[33]. Do experiences, encoded by neuronal activity, influence myelination? Mice reared in social isolation from postnatal days 21–35 show altered prefrontal cortex myelination that corresponds with deficits in social interactions and working memory[14]. This critical period for experience-dependent myelination corresponds with cortical oligodendrocyte maturation and axon ensheathment, suggesting that experience and neuronal activity may alter the behavior of myelinating oligodendrocytes. Our findings that activity-dependent secretion from axons regulates myelin sheath growth, stabilization, and axon selection provide a basis for the stereotyped selection of specific axons, and how altered experience can change the myelinogenic landscape.

METHODS

Zebrafish lines and husbandry

All animal work performed in this study was approved by the Institutional Animal Care and Use Committee at the University of Colorado School of Medicine. Zebrafish embryos were raised at 28.5°C in egg water and staged according to hours post-fertilization or morphological criteria. *Tg(sox10:mRFP)^{vu234}*, *Tg(olig2:EGFP)^{vu1}*, *Tg(phox2B:GFP)^{w37}*[34], *Tg(sox10:GAL4-VP16, cmlc2:Cerulean)^{co19}*, *Tg(mbp:GAL4-VP16, cmlc2:Cerulean)^{co20}*, *Tg(phox2B:GAL4-VP16, cmlc2:Cerulean)^{co21}*, *Tg(4xnrUAS:EGFP-CaaX, cmlc2:EGFP)^{co18}*, *Tg(4xnrUAS:mCherry-CaaX, clmc2:EGFP)^{co22}*, *Tg(neuroD:TeNT-GFP)^{co23}*, *Tg(UAS:Synaptophysin-GFP)* (ref[35]), and *Tg(UAS:ChRWR-EGFP)/js3* (ref. 23) transgenic zebrafish strains were used in this study. *Tg(neuroD:TeNT-GFP)^{co23}* zebrafish are paralyzed, unable to feed or form a swim bladder, and therefore not viable past one week. Therefore, all experiments using this line were performed in the F1 generation.

Plasmid construction and generation of new transgenic zebrafish

The GAL4 lines *Tg(sox10:GAL4-VP16, cmlc2:Cerulean)*^{co19}, *Tg(mbp:GAL4-VP16, cmlc2:Cerulean)*^{co20}, *Tg(phox2B:GAL4-VP16, cmlc2:Cerulean)*^{co21} were created by injecting Tol2 DNA plasmids, together with Tol2 mRNA, into one-cell embryos. GAL4 DNA plasmids were created by Gateway cloning into the Tol2 expression plasmid *pCH-Tol2-Gtwy-GAL4-VP16* (gift from Michael Nonet). For *pEXPR-Tol2-sox10:GAL4-VP16, cmlc2:cerulean*, we used an entry plasmid containing a 7.2 kb genomic fragment of zebrafish *sox10* (ref. 36). *For pEXPR-Tol2-mbp:GAL4-VP16, cmlc2:cerulean*, we used an entry plasmid containing a 2.6 kb genomic fragment of zebrafish *mbp-a*. Primers are described elsewhere[37]. For *pEXPR-Tol2-phox2Bb:GAL4-VP16, cmlc2:cerulean*, we used an entry plasmid containing a 2.1 kb genomic fragment of zebrafish *phox2bb*. Primer sequences were 5' GCTGAATTTTTACAGGTTTAAAAGAGG and 5' TCATTCAAACAGTAATATCAAAGGTTTC. We used multi-site gateway cloning to construct *pEXPR-Tol2-4xnrUAS:EGFP-CaaX, cmlc2:EGFP, pEXPR-Tol2-4xnrUAS:mCherry-CaaX, cmlc2:EGFP, pEXPR-Tol2-mbp:TagRFP-T, and pEXPR-Tol2-sox10:TagRFP-T*. Entry clones were derived from the Tol2kit system[38]. *pEXPR-Tol2-neuroD:TeNT-GFP* was created using multi-site gateway cloning. The 5' entry plasmid contained a 5 kb genomic fragment of zebrafish *neuroD* (ref. 39). The middle entry plasmid contained TeNT-GFP fusion protein, which was subcloned from *pCS2+TeNT-LC:EGFP*, a gift from Martin Meyer, using EcoRI and NotI restriction enzymes. This fusion protein has been extensively characterized and potently inhibits evoked exocytosis in zebrafish neurons in vivo[16].

Antibody labeling

To immunolabel MBP in *Tg(phox2B:GFP)* larvae, we fixed 7 dpf larvae in paraformaldehyde buffer and generated transverse sections using routine methods. Rabbit anti-MBP (1:200 dilution, generated commercially against the peptide sequence CSRSRSPPKRWSTIF, Open Biosystems)[40] and goat anti-rabbit AlexaFluor 568 (10 μg/ml, Life Technologies) antibodies were applied to transverse sections. Labeling with rabbit anti-Sox10 has been previously described[41].

Drug treatments

We injected 2 nL tetrodotoxin (EMD, 0.5 mM) directly into the yolk of 48 hpf larvae. This concentration consistently paralyzed larva for at least three days. Our initial experiments showed that concentrations greater than 0.5 mM compromised cardiac function, suggesting inhibition of TTX-resistant channels. We injected TTX in a buffered solution containing 0.05% phenol red, 120 mM KCl, 30 mM Hepes, pH adjusted 7.3. Control larvae were injected with a vehicle solution containing injection solution. Veratridine (Sigma-Aldrich V5754) stock was prepared by dissolving in EtOH to 10mM. We injected 2 nL veratridine (1 mM in 0.4M KCl) into the yolk of 72 hpf embryos and selected embryos with a touch response phenotype at 96 hpf for confocal imaging.

Microscopy and Image Analysis

For static imaging of single time points, we embedded larvae for lateral views of the spinal cord in 1% low-melt agarose containing tricaine. We acquired all confocal images using a Zeiss LSM 780 (Carl Zeiss) or a Zeiss Axiovert 200 microscope equipped with a PerkinElmer spinning disk confocal system (PerkinElmer Improvision) with 40× 1.3 NA oil immersion or 63× 1.2 NA water immersion objectives. We used Zen (Carl Zeiss) or Volocity (PerkinElmer) softwares for image acquisition, and ImageJ (National Institutes of Health) for image analysis and processing.

To analyze wrapping of axons marked by *Tg(phox2B:GFP)*, we collected images of 96–100 hpf larvae at somites 27–30 and oversampled z-stacks (0.3 μm intervals) to maximize z-resolution. We measured the number and length of all nascent sheaths ventral to, but not including the Mauthner axon. Sheaths were assigned as wrapping GFP^+ or GFP^- axons, and we used orthogonal views to inspect all planes in order to confirm assignments. For imaging of axon selection marked by *UAS*-driven expression in *Tg(phox2B:GAL4)* larvae, we collected images of 96–100 hpf larvae at somites 21–23. Percent length measurements were made by measuring the length of all sheaths wrapping a single axon and dividing by the total length of the axon in the field of view.

For experiments measuring the number and length of myelin segments emanating from single oligodendrocytes, we injected *UAS*:mCherry-CaaX plasmids into *Tg(mbp:GAL4)* or *Tg(sox10:GAL4)* blastomeres. We also analyzed scatter-labeled oligodendrocytes in *Tg(mbp:GAL4)*; *Tg(UAS:mCherry-CaaX)* double positive larvae. This mosaicism is most likely a consequence of *UAS* transgene silencing in zebrafish. To ensure that all myelin segments emanated from a single soma, and not neighboring oligodendrocytes, we only imaged and analyzed isolated oligodendrocytes with no labeled cells in adjacent segments.

To determine the number of oligodendrocyte progenitor cells (OPCs) we used the *Tg(olig2:EGFP)* reporter line. After chemical fixation and embedding we generated transverse sections of spinal cord. Routine immunofluorescence protocols were used to label $Sox10^+$ spinal cord cells using rabbit anti-Sox10 and goat anti-rabbit Alexa 568 secondary antibodies. We then counted the number of *olig2:*$EGFP^+$ $Sox10^+$ cells per transverse section in the anterior spinal cord. The average OPC number per fish was generated from 10 independent sections. Cell counts were performed using a Zeiss Axiovert 200 microscope equipped with mercury arc lamp and a 20× 0.8 NA objective.

To determine the number of oligodendrocytes we used the *Tg(mbp:EGFP)* reporter line. Images were collected using the PerkinElmer spinning disk confocal and the number of oligodendrocytes per field was quantified within Volocity software. Only cells with fluorescence intensities two-fold greater than the mean background pixel intensity were counted in analysis.

To determine the number of OPCs and oligodendrocytes in *Tg(neuroD:TeNT-GFP)* larvae we crossed to either *Tg(sox10:TagRFP-T)* or *Tg(mbp:TagRFP-T)* reporter lines. Images were collected using the PerkinElmer spinning disk confocal. Confocal stacks at multiple

segments were acquired and tiled to generate a large field spanning 1 mm along the anterior-posterior axis. Cell counts were performed within Volocity software.

Time-lapse imaging

All fluorescence time-lapse imaging was performed on the spinning disk confocal system equipped with a heated stage chamber to maintain larvae at 28.5°C. Larvae were paralyzed by immersion in 0.5 mg/ml α-Bungarotoxin (EMD) in 10% Hank's solution, aided by a small incision in the caudal-most tail epidermis with a fine tungsten needle. After 10-min incubation in α-Bungarotoxin, larvae recovered in egg water without anesthetic for at least 1-hr. Paralyzed larvae were then embedded in 1% low-melt agarose, without tricaine, and immersed in egg water without tricaine. For time-lapse imaging of initial ensheathment, we collected images at 2.5 min intervals for 4 hr. Analysis of sheath initiation was performed by a blind observer. Nascent sheaths were defined morphologically by identifying two parallel *sox10:*mRFP$^+$ membrane processes extending longitudinally along the anterior-posterior axis with lengths exceeding 1 μm. We acquired images at 20 min intervals for retraction assays. When time-lapse durations exceeded 18 hr, we recovered larva to egg water without tricaine, then re-embedded in low-melt agarose immediately prior to the next time point. Time-lapse videos were exported from Volocity as extended z-projection TIFF images. We used ImageJ to rotate, crop, and translate in order to correct for x-y drift. Image stacks were then exported in QuickTime (.mov) format using Sorensen 3 compression.

Swim behavior in veratridine-treated larvae

To assess behavioral phenotypes we used a standard touch assay on 3 dpf larvae. A pin tool was used to induce the touch response and any larva with movement persisting greater than 5 sec and terminating in seizure-like activity was scored as positive. We collected representative time-lapse videos using a Samsung Galaxy S3 digital camera with 8 megapixel and 30 frames per second acquisition settings. Videos were exported in .mov format within QuickTime Pro 7 using H.264 compression.

Optogenetic stimulation and analysis

We crossed *Tg(phox2B:GAL4; cmlc2:Cerulean)*; *Tg(sox10:mRFP)* × *Tg(UAS:ChRWR-EGFP)/js3* adults. At 72 hpf, embryos positive for EGFP$^+$ axons and *sox10*:mRFP were split into control and treated groups. Blue (473 nm, 20 Hz) light was delivered using a Blues 50 laser (473 nm, 3 mW/cm^2, Cobolt Inc., San Jose, CA, USA) controlled by a Uniblitz shutter (Vincent Associates, Rochester, NY, USA) and LabView software v. 2012 (National Instruments, Austin, TX, USA). We applied 30 sec pulses (20 Hz) every 2 min for a total of 3 hr. To assess selection of phox2B$^+$ axons we performed confocal microscopy 24 hr post-stimulation. Images were acquired at the somite position corresponding to where axon wrapping was initiating at the time of treatment (as determined by confocal microscopy).

Electron Microscopy

To measure axon size, we fixed 3 dpf *Tg(neuroD:TeNT-GFP)* larvae and siblings from 2 clutches in 2% paraformaldehyde, 2% glutaraldehyde and 0.1M sodium cacodylate. Microwave stimulation to accelerate fixation of tissue was performed with a Biowave Pro

Laboratory Microwave with ColdSpot (Ted Pella, Inc., Redding, CA, USA) maintained at 15°C. Membranes were enhanced using secondary fixation with OsO_4. We collected the electron micrographs using a FEI Techai G2 BioTwin microscope and images were cropped and contrast-adjusted in Adobe Photoshop. We analyzed 4–5 cross-sections of tissue between somites 12–14 for each of 3 larvae per condition. On each cross-section, an unbiased observer randomly selected 5 to 10 axons ventral to each Mauthner axon [within a consistent area of 27 μm^2] for a total of 204 sib axons and 185 axons from *Tg(neuroD:TeNT-GFP)* embryos. Axons were chosen without regard to myelination and were required to have a clearly defined perimeter. The axon area was measured in ImageJ and the axon diameter was calculated from the area value.

Statistical analyses

We plotted all data and performed all statistical analyses within GraphPad Prism software (v6). All data are expressed as mean ± SEM. For statistical analysis, we first performed the D'Agonstino and Pearson omnibus normality test to address normality. We used Student's two-tailed *t*-test for all data with normal distribution. For all other data, we assessed statistical significance using the nonparametric Mann-Whitney test. Statistical significance is indicated as follows: $*P < 0.05$, $**P < 0.01$, $***P < 0.001$. No statistical methods were used to pre-determine sample sizes but our sample sizes are similar to those reported in previous publications[7,9,24]. A supplementary methods checklist is available.

Supplementary Material

Refer to Web version on PubMed Central for supplementary material.

Acknowledgments

We are grateful to Anthony J. Treichel (Winona State University) for help with image analysis. We thank Alex Nechiporuk (Oregon Health Sciences University) for *Tg(phox2B:EGFP)* zebrafish, Hiromu Yawo (Tohoku University) and the National BioResource Zebrafish Project for *Tg(UAS:ChRWR-EGFP)* zebrafish, Martin Meyer (King's College London) for the *pCS2-TeNT-GFP* plasmid, and Joseph Fetcho (Cornell University) for the *UAS:hKir2.1-2A-EGFP-CaaX* plasmid. We thank Mary Goll (Memorial Sloan-Kettering Cancer Center), Michael Nonet (Washington University), Chi-Bin Chien (University of Utah), and Kristen Kwan (University of Utah) for Gateway plasmids. For critical feedback on the project, we thank Matthew Rasband (Baylor University), Jason Triplett (Children's National Medical Center), Steven Henle (Harvard University), Angie Ribera (University of Colorado School of Medicine) and Wendy Macklin (University of Colorado School of Medicine) and all members of the Appel, Ribera, and Macklin laboratories. We also thank Jamie Costabile (University of Colorado School of Medicine) and the University of Colorado Anschutz Medical Campus Optogenetics Core Facility for assistance with *UAS:ChRWR-EGFP* experiments. This work was supported by NIH Grant R01 NS046668 and a gift from the Gates Frontiers Fund to B.A., National Multiple Sclerosis Postdoctoral Fellowship (FG 2024-A-1), National Institutes of Health (NIMH) T32 MN015442 Fellowship to J.H.H. and National Institutes of Health (NCI) T32 5T32CA08208613 Fellowship to A.M.R. The University of Colorado Anschutz Medical Campus Zebrafish Core Facility is supported by NIH grant P30 NS048154. All DNA plasmids and transgenic zebrafish used in this study are available by request.

References

1. Sturrock RR. Myelination of the mouse corpus callosum. Neuropathol. Appl. Neurobiol. 1980; 6:415–420. [PubMed: 7453945]
2. Rosenberg SS, Kelland EE, Tokar E, la Torre De AR, Chan JR. The geometric and spatial constraints of the microenvironment induce oligodendrocyte differentiation. Proc Natl Acad Sci USA. 2008; 105:14662–14667. [PubMed: 18787118]

3. Lee S, et al. A culture system to study oligodendrocyte myelination processes using engineered nanofibers. Nat Methods. 2012; 9:917–922. [PubMed: 22796663]
4. Gyllensten L, Malmfors T. Myelinization of the optic nerve and its dependence on visual function--a quantitative investigation in mice. J Embryol Exp Morphol. 1963; 11:255–266. [PubMed: 13963537]
5. Tauber H, Waehneldt TV, Neuhoff V. Myelination in rabbit optic nerves is accelerated by artificial eye opening. Neurosci Lett. 1980; 16:235–238. [PubMed: 6302574]
6. Demerens C, et al. Induction of myelination in the central nervous system by electrical activity. Proc Natl Acad Sci USA. 1996; 93:9887–9892. [PubMed: 8790426]
7. Wake H, Lee PR, Fields RD. Control of local protein synthesis and initial events in myelination by action potentials. Science. 2011; 333:1647–1651. [PubMed: 21817014]
8. Barres BA, Raff MC. Proliferation of oligodendrocyte precursor cells depends on electrical activity in axons. Nature. 1993; 361:258–260. [PubMed: 8093806]
9. Gibson EM, et al. Neuronal activity promotes oligodendrogenesis and adaptive myelination in the mammalian brain. Science. 2014; 344:1252304–1252304. [PubMed: 24727982]
10. Kukley MM, Capetillo-Zarate EE, Dietrich DD. Vesicular glutamate release from axons in white matter. Nat Neurosci. 2007; 10:311–320. [PubMed: 17293860]
11. Ziskin JL, Nishiyama A, Rubio M, Fukaya M, Bergles DE. Vesicular release of glutamate from unmyelinated axons in white matter. Nat Neurosci. 2007; 10:321–330. [PubMed: 17293857]
12. Ng BKB, Chen LL, Mandemakers WW, Cosgaya JMJ, Chan JRJ. Anterograde transport and secretion of brain-derived neurotrophic factor along sensory axons promote Schwann cell myelination. Journal of Neuroscience. 2007; 27:7597–7603. [PubMed: 17626221]
13. Káradóttir R, Attwell D. Neurotransmitter receptors in the life and death of oligodendrocytes. Neuroscience. 2007; 145:1426–1438. [PubMed: 17049173]
14. Makinodan M, Rosen KM, Ito S, Corfas G. A critical period for social experience-dependent oligodendrocyte maturation and myelination. Science. 2012; 337:1357–1360. [PubMed: 22984073]
15. Liu J, et al. Impaired adult myelination in the prefrontal cortex of socially isolated mice. Nat Neurosci. 2012; 15:1621–1623. [PubMed: 23143512]
16. Ben Fredj N, et al. Synaptic activity and activity-dependent competition regulates axon arbor maturation, growth arrest, and territory in the retinotectal projection. J Neurosci. 2010; 30:10939–10951. [PubMed: 20702722]
17. Agetsuma MM, et al. The habenula is crucial for experience-dependent modification of fear responses in zebrafish. Nat Neurosci. 2010; 13:1354–1356. [PubMed: 20935642]
18. Hua JY, Smear MC, Baier H, Smith SJ. Regulation of axon growth in vivo by activity-based competition. Nature. 2005; 434:1022–1026. [PubMed: 15846347]
19. McLaughlin T, Torborg CL, Feller MB, O'Leary DDM. Retinotopic map refinement requires spontaneous retinal waves during a brief critical period of development. Neuron. 2003; 40:1147–1160. [PubMed: 14687549]
20. Nicol X, et al. cAMP oscillations and retinal activity are permissive for ephrin signaling during the establishment of the retinotopic map. Nat Neurosci. 2007; 10:340–347. [PubMed: 17259982]
21. Plazas PV, Nicol X, Spitzer NC. Activity-dependent competition regulates motor neuron axon pathfinding via PlexinA3. Proc Natl Acad Sci USA. 2013; 110:1524–1529. [PubMed: 23302694]
22. Kishore S, Fetcho JR. Homeostatic regulation of dendritic dynamics in a motor map in vivo. Nat Commun. 2013; 4:2086. [PubMed: 23803587]
23. Umeda K, et al. Targeted expression of a chimeric channelrhodopsin in zebrafish under regulation of Gal4-UAS system. Neurosci Res. 2013; 75:69–75. [PubMed: 23044184]
24. Czopka T, ffrench-Constant C, Lyons DA. Individual oligodendrocytes have only a few hours in which to generate new myelin sheaths in vivo. Dev Cell. 2013; 25:599–609. [PubMed: 23806617]
25. Colello RJ, Pott U, Schwab ME. The role of oligodendrocytes and myelin on axon maturation in the developing rat retinofugal pathway. Journal of Neuroscience. 1994; 14:2594–2605. [PubMed: 7514208]

26. Sánchez I, Hassinger L, Paskevich PA, Shine HD, Nixon RA. Oligodendroglia regulate the regional expansion of axon caliber and local accumulation of neurofilaments during development independently of myelin formation. Journal of Neuroscience. 1996; 16:5095–5105. [PubMed: 8756439]
27. Almeida RG, Lyons DA. On the resemblance of synapse formation and CNS myelination. Neuroscience. 2013
28. McKenzie IA, et al. Motor skill learning requires active central myelination. Science. 2014; 346:318–322. [PubMed: 25324381]
29. Shrager P, Novakovic SD. Control of myelination, axonal growth, and synapse formation in spinal cord explants by ion channels and electrical activity. Brain Res Dev Brain Res. 1995; 88:68–78. [PubMed: 7493408]
30. De Biase LM, et al. NMDA receptor signaling in oligodendrocyte progenitors is not required for oligodendrogenesis and myelination. J Neurosci. 2011; 31:12650–12662. [PubMed: 21880926]
31. Káradóttir R, Hamilton NB, Bakiri Y, Attwell D. Spiking and nonspiking classes of oligodendrocyte precursor glia in CNS white matter. Nat Neurosci. 2008; 11:450–456. [PubMed: 18311136]
32. Chittajallu R, Aguirre A, Gallo V. NG2-positive cells in the mouse white and grey matter display distinct physiological properties. J Physiol (Lond). 2004; 561:109–122. [PubMed: 15358811]
33. Fields RD. White matter in learning, cognition and psychiatric disorders. Trends Neurosci. 2008; 31:361–370. [PubMed: 18538868]
34. Nechiporuk A, Linbo T, Poss KD, Raible DW. Specification of epibranchial placodes in zebrafish. Development. 2007; 134:611–623. [PubMed: 17215310]
35. Heap LA, Goh CC, Kassahn KS, Scott EK. Cerebellar output in zebrafish: an analysis of spatial patterns and topography in eurydendroid cell projections. Front Neural Circuits. 2013; 7:53–53. [PubMed: 23554587]
36. Kucenas S, et al. CNS-derived glia ensheath peripheral nerves and mediate motor root development. Nat Neurosci. 2008; 11:143–151. [PubMed: 18176560]
37. Jung S-H, et al. Visualization of myelination in GFP-transgenic zebrafish. Dev Dyn. 2010; 239:592–597. [PubMed: 19918882]
38. Kwan KM, et al. The Tol2kit: a multisite gateway-based construction kit for Tol2 transposon transgenesis constructs. Dev Dyn. 2007; 236:3088–3099. [PubMed: 17937395]
39. Mo W, Nicolson T. Both pre- and postsynaptic activity of Nsf prevents degeneration of hair-cell synapses. PLoS ONE. 2011; 6:e27146. [PubMed: 22073277]
40. Kucenas S, Wang W-D, Knapik EW, Appel B. A selective glial barrier at motor axon exit points prevents oligodendrocyte migration from the spinal cord. J Neurosci. 2009; 29:15187–15194. [PubMed: 19955371]
41. Park H-C, Boyce J, Shin J, Appel B. Oligodendrocyte specification in zebrafish requires notch-regulated cyclin-dependent kinase inhibitor function. J Neurosci. 2005; 25:6836–6844. [PubMed: 16033893]

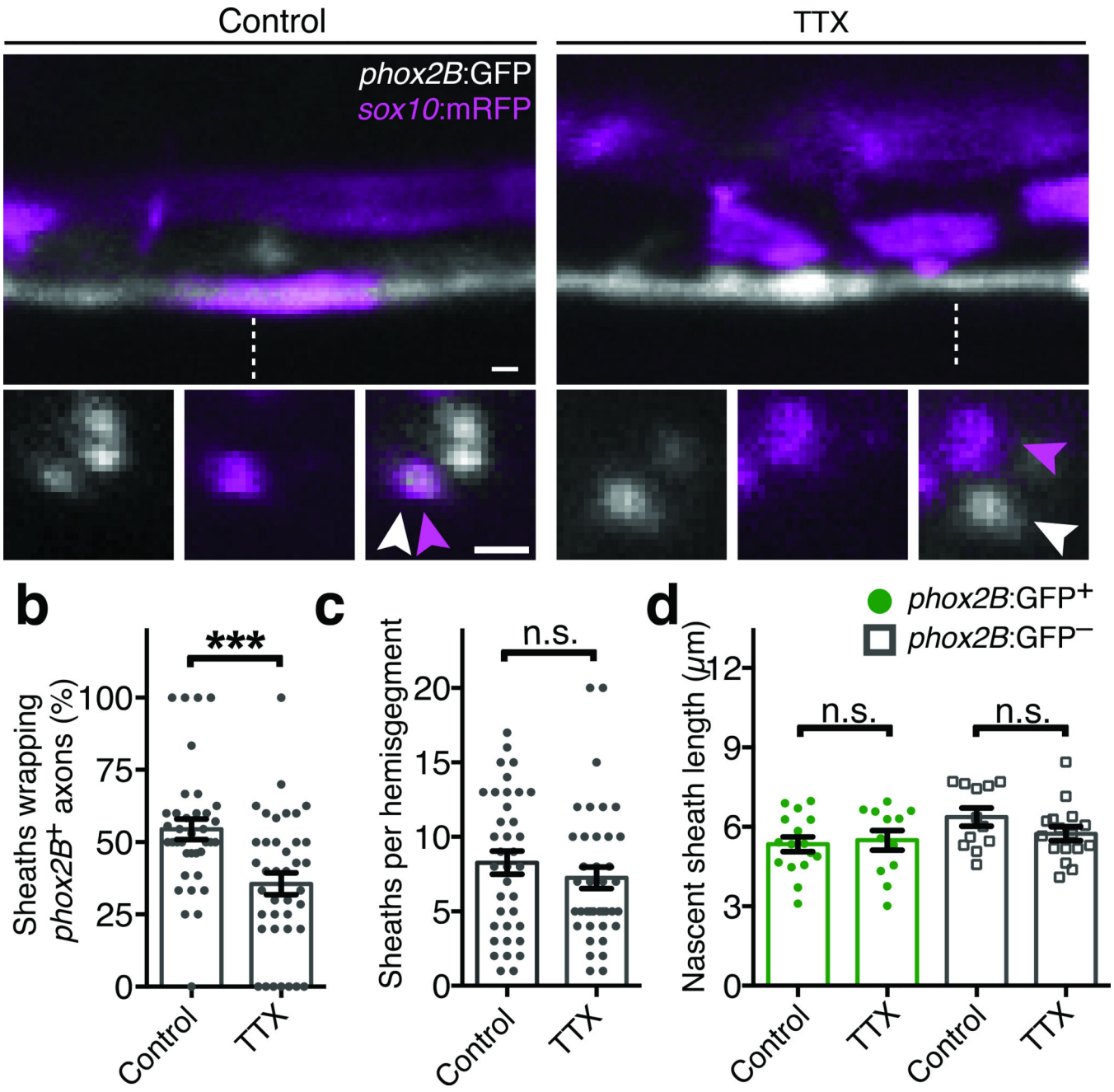

Figure 1. Axon selection is biased by electrical activity

(**a**) Confocal images show axon wrapping in *Tg(phox2B:GFP)* larvae. In control larvae (left), *phox2B*$^{+}$ axons are frequently wrapped by nascent myelin sheaths marked by *sox10:*mRFP. TTX treatment (right) reduces the proportion of nascent sheaths wrapping *phox2B*$^{+}$ axons. For each condition, the upper panels are lateral spinal cord views and the lower panels show orthogonal projections, which were generated at the dashed lines. Arrowheads point to axons (white) and nascent sheaths (magenta). Scale bars, 1 μm. (**b**) Quantification of the proportion of *sox10*:mRFP sheaths wrapping *phox2B*$^{+}$ axons. P = 0.0005, *t*-test. (**c**) Quantification of the overall number of nascent sheaths per spinal cord

hemisegment. $P = 0.3426$, *t*-test. For (b–c), $n = 22$ control larvae (283 sheaths) and 23 TTX-treated larvae (283 sheaths). (**d**) Quantification of nascent sheath length; $n = 16$ control larvae (406 sheaths) and 12 TTX-treated larvae (296 sheaths). $P = 0.7468$ (*phox2B*:GFP$^+$) and $P = 0.1540$ (*phox2B*$^-$), *t*-test. For all panels, error bars show s.e.m.; ***$P < 0.001$; n.s., not significant.

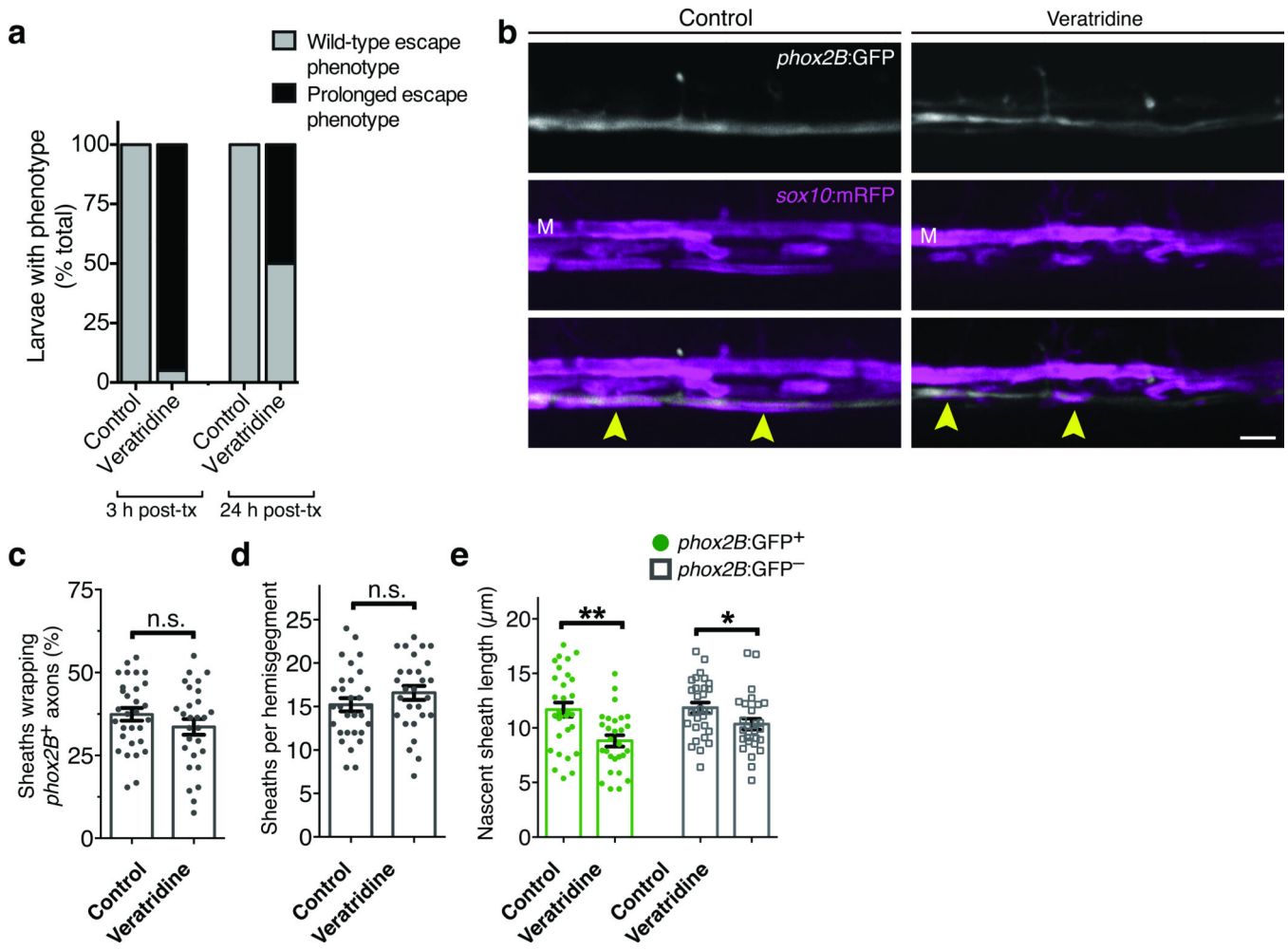

Figure 2. Veratridine reduces nascent sheath length but not sheath number or axon selection

(**a**) Quantification of touch response assays on control and veratridine-treated larvae. Data shown represent the proportion of larvae exhibiting either wild-type or prolonged touch-response phenotypes (see Methods). Scoring was performed three hours after treatment and again immediately prior to confocal imaging (24 hr post-treatment). For both control and treated groups, $n = 80$ (3 h post-treatment) and 76 (24 h post-treatment). (**b**) Representative confocal images show reporter expression in control and veratridine-treated *Tg(phox2B:GFP); Tg(sox10:mRFP)* larvae. M indicates the position of the Mauthner axon and arrowheads point to sites of *phox2B*$^+$ axon wrapping. Scale bar, 5 μm. (**c–e**) Summary of axon selection, sheath number, and sheath length measurements from (b). Error bars show s.e.m.; *t*-test; $*P < 0.05$, $**P < 0.01$; n.s., not significant. For (c–e) $n = 30$ control and 28 veratridine-treated larvae. $P = 0.2147$ (c), $P = 0.2173$ (d), $P = 0.0011$ (e, left), and $P = 0.0342$ (e, right); *t*-test.

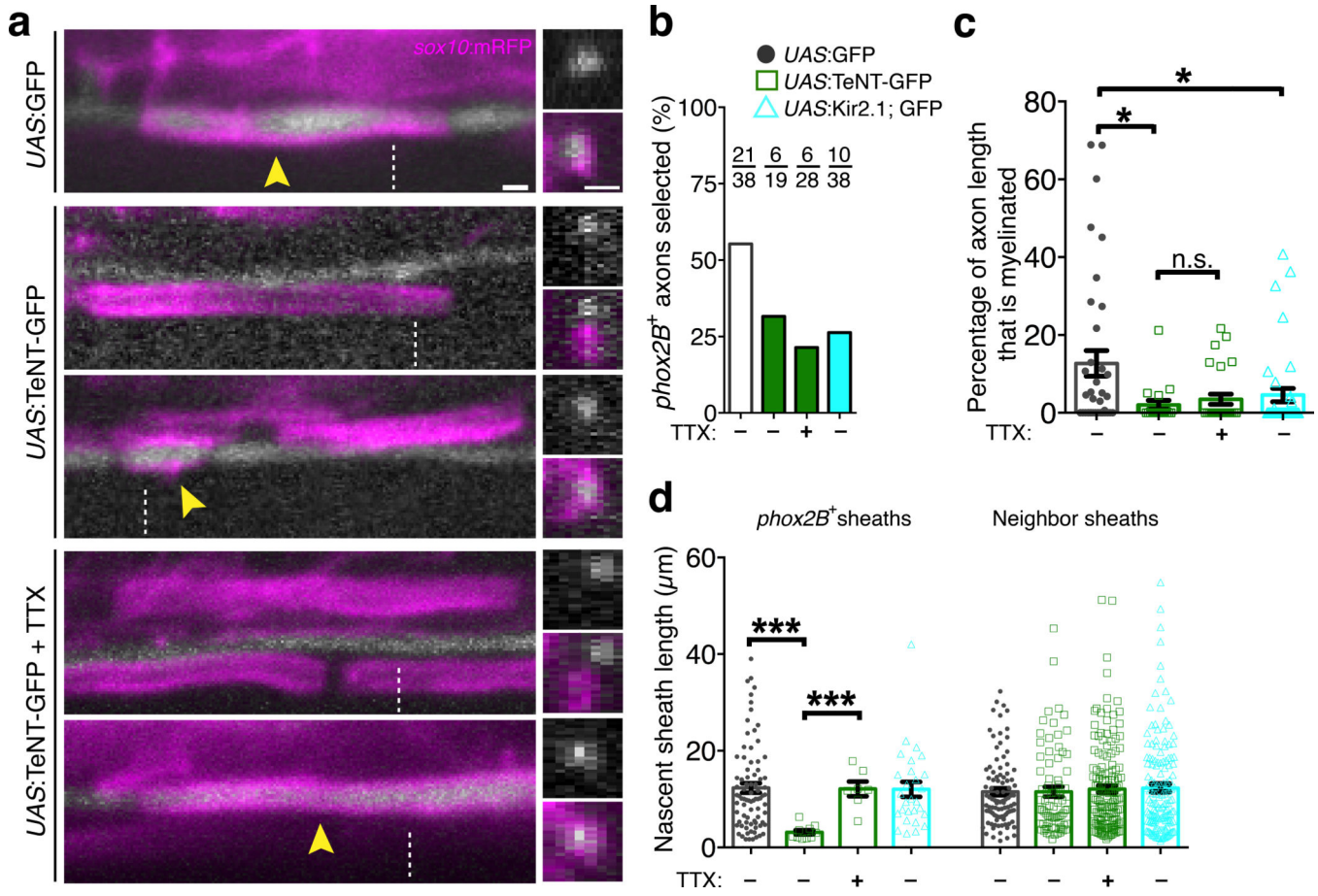

Figure 3. Activity-dependent competition during axon selection

(**a**) Confocal images show expression of *UAS*:GFP or *UAS*:TeNT-GFP in single *phox2B*$^{+}$ axons and nascent sheaths marked by *sox10*:mRFP. Images on the left are lateral views and the right panel shows orthogonal projections, generated at the dashed lines. Arrowheads point to ensheathed axons. Scale bars, 1 μm. (**b**) Summary of the percentage of axons selected for myelination. For each condition, the number selected and overall number of axons analyzed is indicated. (**c**) Quantitative measurements show the wrapping efficiency of *phox2B*$^{+}$ axons expressing from the indicated plasmids. Data are expressed as the percent of total axon length ensheathed at the time of imaging. $P = 0.0096$ (upper asterisk), $P = 0.0294$ (lower asterisk), $P = 0.7257$ (lower comparison, n.s.), Mann-Whitney test. (**d**) Quantification of nascent sheath length. Left bars show the average length of sheaths wrapping GFP^{+} axons, and the right bars show lengths of nascent sheaths wrapping neighboring, unmarked axons in the same larvae. $P < 0.0001$ (left comparison), $P = 0.0002$ (right comparison), Mann-Whitney test. For (c–d), *n* corresponds to the numbers of axons indicated in (b) derived from 17 (*UAS*:GFP), 17 (*UAS*:TeNT-GFP), 22 (*UAS*:TeNT-GFP + TTX), and 29 (*UAS*:Kir2.1; EGFP) larvae. Error bars show s.e.m.; *$P < 0.05$, ***$P < 0.001$; n.s., not significant.

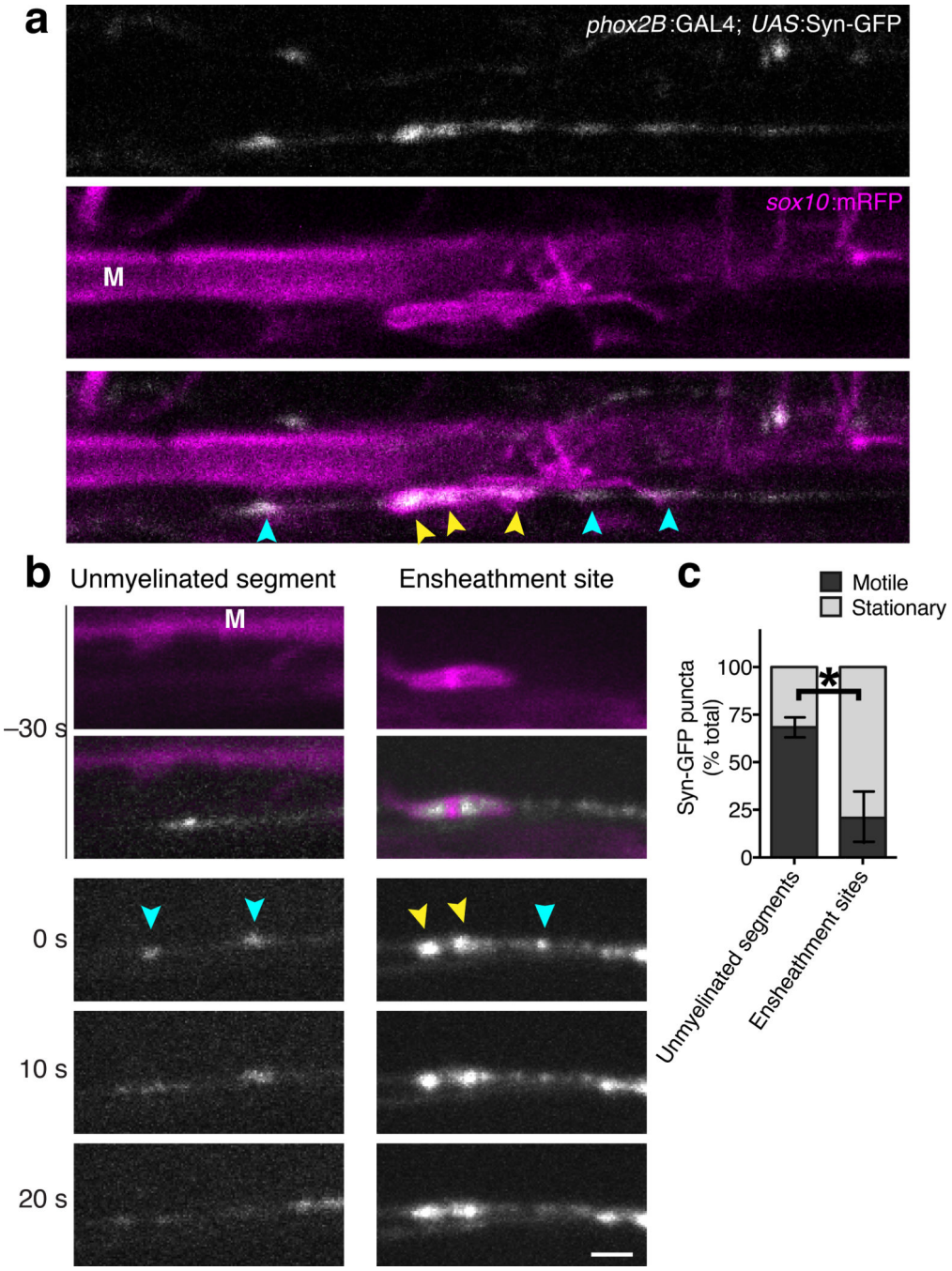

Figure 4. Accumulation of Syn-GFP vesicles at myelin ensheathment sites

(**a**) Representative confocal images show Syn-GFP vesicle puncta (white) and nascent myelin sheaths marked by the *sox10*:mRFP reporter (magenta). (**b**) Representative time-lapse confocal images show stationary and motile Syn-GFP^{+} vesicle puncta at unmyelinated axon segments (left panels) and ensheathment sites (right panels). The upper panels show images acquired 30 s prior to the onset of time-lapse imaging, and the lower panels show time-lapse images acquired at 10 s intervals. For (a–b), Syn-GFP puncta at unmyelinated segments and ensheathment sites are indicated by blue and yellow arrowheads, respectively.

Images are lateral views with dorsal up and anterior right. The Mauthner axon (M) is marked for reference. Scale bars, 2 μm. (**c**) Summary of vesicle motility measurements show the proportion of motile and stationary vesicles at unmyelinated segments and ensheathment sites. Error bars represent s.e.m.; $n = 272$ puncta at unmyelinated segments (12 larvae), 31 puncta at ensheathment sites (7 larvae); ***$P = 0.0009$, *t*-test.

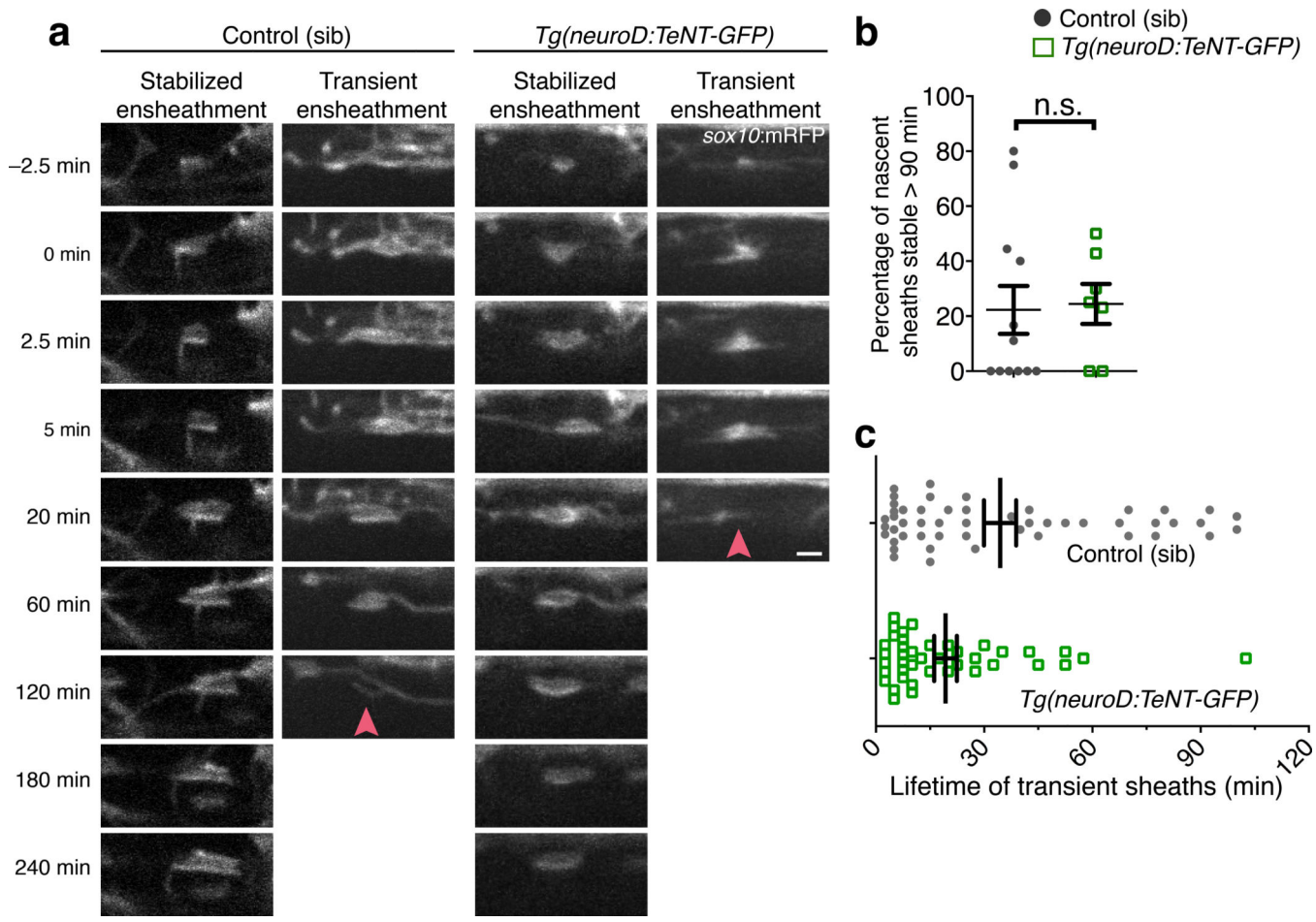

Figure 5. Activity-dependent secretion is not required for initial axon wrapping

(**a**) Representative time-lapse confocal images show initiation of axon wrapping in the ventral spinal cord of sibling control (left panels) and *Tg(neuroD:TeNT-GFP)* larvae (right panels). Images are lateral views and time (min) relative to wrapping initiation is indicated at the left. Arrowheads point to prospective sheaths that fail to stabilize. Scale bar, 2 μm. (**b**) Summary of time-lapse measurements show the proportion of prospective sheaths that are stable for at least 90 min. *n* = 12 control (66 sheaths) and 8 TeNT-GFP larvae (57 sheaths); *P* = 0.5624, Mann-Whitney test. (**c**) Measurements of nascent sheath lifetime amongst transient ensheathments during time-lapse imaging in (a). *n* = 12 control (50 prospective sheaths) and 8 TeNT-GFP larvae (41 prospective sheaths); *P* = 0.0411, Mann-Whitney test. For (b–c), error bars show s.e.m., **P* < 0.05; n.s., not significant.

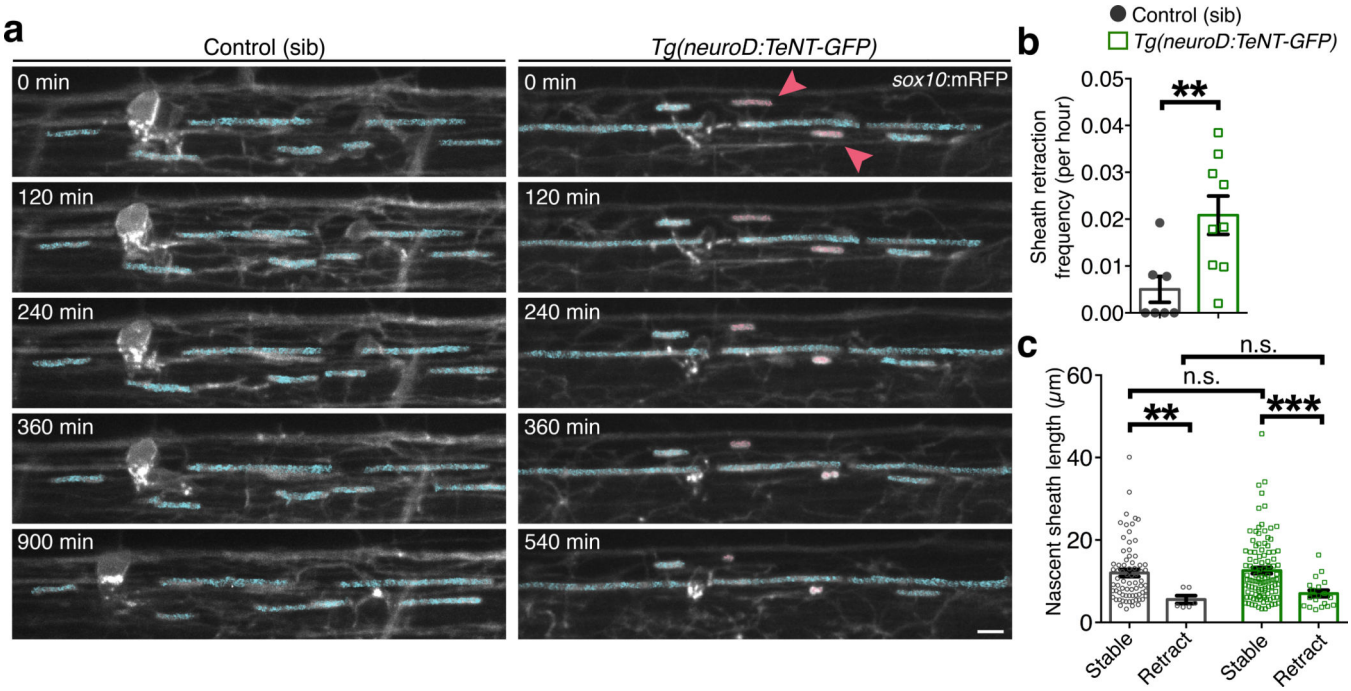

Figure 6. Nascent myelin sheaths are stabilized by activity-dependent secretion

(**a**) Representative confocal images show the retraction of existing sheaths during 15-hr time-lapse imaging in sibling control and *Tg(neuroD:TeNT-GFP)* larvae. Images are lateral views of the dorsal spinal cord and the time (min) relative to the start of image acquisition is indicated for each image. For demonstrative purposes, sheaths stable for the entire time-lapse are shaded in blue and retracting sheaths are shaded red. Scale bar, 5 μm. (**b**) Summary of time-lapse measurements show the frequency of sheath retraction. n = 7 control (99 sheaths) and 9 *Tg(neuroD:TeNT-GFP)* larvae (129 sheaths). P = 0.0071, Mann-Whitney test. (**c**) Quantitative measurements show the relationship between sheath length and stability. Bars represent the mean ± s.e.m. n = 7 control larvae (72 stable sheaths, 6 retracting sheaths) and 9 *Tg(neuroD:TeNT-GFP)* larvae (106 stable sheaths, 19 retracting sheaths). P = 0.0034 (left, **), P = 0.0002 (right, ***), P = 0.3737 (upper n.s.), P = 0.6105 (lower n.s.), Mann-Whitney test; For (b–c), $^{**}P < 0.01$, $^{**}P < 0.001$.